N-methyl-D-glucamine based cryogels as reusable sponges to enhance heavy metals removal from water

Tommaso Mecca[a], Martina Ussia[*b], Daniele Caretti[c], Francesca Cunsolo[a], Sandro Dattilo[d], Stefano Scurti[c], Vittorio Privitera[b], Sabrina C. Carroccio [b,d]

[a] *CNR-ICB, Via Paolo Gaifami 18, 95126, Catania, Italy.*

[b] *CNR-IMM, Via Santa Sofia 64, 95123, Catania, Italy.*

[c] *Industrial Chemistry "Toso Montanari" Department, University of Bologna, Viale Risorgimento 4, 40136, Bologna, Italy.*

[d]*CNR-IPCB, Via Paolo Gaifami 18, 95126, Catania, Italy.*

Keywords: *adsorption, hydrogel, heavy metal, N-methyl-D-glucamine, isotherm.*

*Correspondence to martina.ussia@ct.infn.it

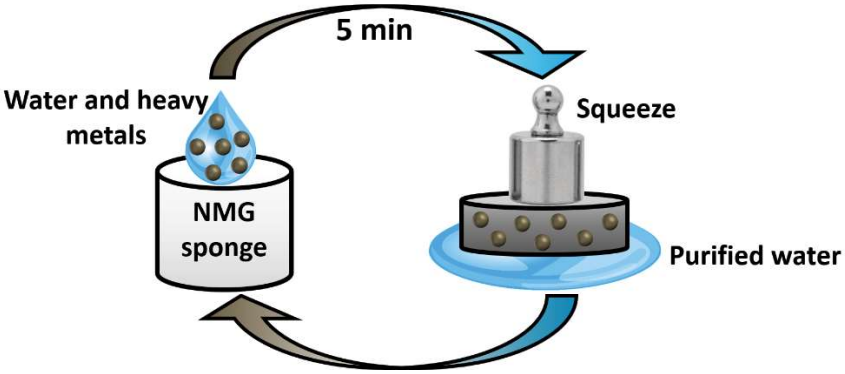

Authors contribution: *S. C. Carroccio and D. Caretti conceived the project idea. D. Caretti and S. Scurti synthetized the monomer performing NMR and FT-IR analyses. M. Ussia and T. Mecca synthesized the cryo-sponges. M. Ussia and T. Mecca performed adsorption tests. T. Mecca carried out porosity tests. M. Ussia achieved, analyzed, and discussed SEM images as well as adsorption, kinetic, and recycling measurements. S. Dattilo and S. C. Carroccio performed and discussed the ICP-MS and TGA measurements. M.Ussia and S. C. Carroccio wrote, reviewed and edited the paper; V. Privitera and F. Cunsolo reviewed and commented on the manuscript at all stages; Sabrina C. Carroccio supervised all work and submission stages.*

Abstract

The design of novel cryogels containing N-methyl-D-glucamine (NMG) group was herein reported. The macroporous materials were prepared via sustainable and feasible cryopolymerization by using as co-monomers (4-vinyl-benzyl)-N-methyl-D-glucamine (VbNMG) and 2-hydroxyethyl methacrylate (HEMA) at different percentages. Particularly, cryogel containing 100% of VbNMG (VbNMG-100) showed excellent ability in fast water uptake, removing arsenic (V) and chromium (VI) metal ions from it. Reusability up to six cycles was also demonstrated. The as-prepared materials were characterized by spectroscopic, thermal, and morphological analyses. The effect of initial oxyanions concentration, kinetic profiles, interfering anions (phosphate and sulphate) were investigated and adsorption/desorption studies were carried out. Equilibrium sorption results well fitted the Langmuir isotherm for both ions tested, showing a startling aptitude in arsenic (76.3 mg/g) as well as chromium (130.9 mg/g) sorption properties if compared with similar polymers as well as

other materials. Exploiting its spongy nature, only 5 mins were needed to absorb contaminated medium releasing purified water by a simple squeezing. Most importantly, the sponge can be easily regenerated and reused again up to three times without the depletion of its efficiency.

1. Introduction

The global demand for access to clean water constitutes one of the urgent challenges to be faced in the next future [1,2]. As pollutants, heavy metals play a major role, since their presence in water sources drastically increased in the past decades, causing serious threat for aquatic and human health. Particularly, arsenic V [As(V)] and chromium VI [Cr(VI)] are included amongst the most hazardous species, so that their level of contamination is strictly regulated by health authorities, recommending a limit content in drinking water of 10 μg/L and 50 μg/L for As(V) and Cr(VI), respectively [3-6]. However, even though these levels are maintained in Europe and the USA, emerging countries' populations are exposed to a considerably higher amount of metal ions in drinking water [6-8]. Indeed, metal contamination in ground and surface waters deriving from anthropogenic activities is scarcely regulated due to missing or unacceptably inadequate environmental control. Therefore, researchers have addressed their efforts in the identification of suitable and cost-effective technologies for their removal [2, 9-22].

As well known, the adsorption is the most widely used technology, consisting in simple and low-cost handling procedures to remove organic and inorganic contaminants from water [2, 23-26] avoiding at the same time the use of chemical reagents as well as the production of harmful by-products downstream [27].

In this context, hydrogels have become a crucial component of novel smart adsorbent materials for several applications including water remediation [15,28-30]. Specifically, hydrogels with a three-dimensional porous structure as well as specific functional moieties (such as carboxylic, amine, hydroxyl, or sulfonic acid groups along their polymeric chains), can trigger the sequestration of metal ions from the contaminated aqueous medium, resulting in stable complexes with them. Hereafter, the linked contaminants can be released from the network by simply changing environmental conditions such as pH, thus regenerating the polymer network. Because of this, together with a desirable increment in terms of efficiency and selectively versus specific elements, these promising materials need to face significant improvements before their transfer into the market, especially in terms of sustainability, as well as chemical and mechanical resistance during the regenerating treatments cycles. As a consequence, cost- and time-saving polymerizations of bio-based as well as synthetic acrylic and vinylic materials functionalized *ad hoc* with chelating groups, was widely reported to achieve resistant and efficient materials. Specifically, huge attention was devoted to the

N-methyl-D-glucamine (NMG) functional moiety due to its high efficiency and selectivity versus metal ions species [31-45]. Indeed, resins containing NMG as a chelating group are already present in the market (e.g. Amberlite® IRA743, DIAION™, and DowexXUS 43594.00).

Monomers containing NMG can be successfully polymerized in situ by radical initiators [31-39]. Alternatively, NMG can be grafted to the material surface after the polymerization step [40-44] by an opportune substitution reaction. Even though this process is feasible from the chemical point of view, the density of NMG loaded cannot reach the 1/1 molar ratio with the monomer concentration. Conversely, a bottom-up approach involves the synthesis of NMG monomers, whose polymerization leads to the final material [31, 34-39]. In this case, the much higher NMG content should ensure superior efficiency to capture metallic species than the grafted ones. However, limitations can arise from the slow and partial diffusion of water into the polymer bulk that can determine the incomplete exploiting of available chelating sites.

Herein, it is reported as a novelty, the syntheses of NMG macroporous hydrogels produced in water by cryo-structuration. Specifically, cryogels were formulated starting from (4-vinyl-benzyl)-N-methyl-D-glucamine (VbNMG) and HEMA monomers. If compared with similar aforementioned materials [31, 35, 39, 41, 42], the macroporous architecture makes the difference.

Indeed, the water-insoluble cryogels complexed the metal ions similarly to other NMG materials since the same chelating agent is used. However, their interconnected macroporous nature provides water fast-diffusion pathways, determining exhaustive access to the chelating sites, thus boosting the ions sequestration.

Besides, it can be used as a sponge providing an interesting adding value. Precisely, after water uptake, the purified medium can be released by simply squeezing it, while contaminants remain entrapped inside. Compared to nanoparticle materials whose excellent adsorption properties derive from the high surface area, freestanding monoliths result safely and easily manageable. Additional benefits can consist also in their lower flow resistance and superior aptitude in filtering heterogeneous solutions without pore obstruction.

In light of these attractive features, syntheses, data related to chemical-physical properties of fabricated sponges as well as As(V) and Cr(VI) uptake, were here proposed, discussed, and compared with those reported in the literature.

2. Experimental part

2.1 Materials

2-Hydroxyethyl methacrylate (HEMA), N, N'-methylene-bis-acrylamide (MBAA), ammonium persulfate (APS), tetramethyl-ethylene-diamine (TEMED), sodium arsenate dibasic heptahydrate

($Na_2HAsO_4 \cdot 7H_2O$), potassium dichromate ($K_2Cr_2O_7$), sodium phosphate dibasic dihydrate ($Na_2HPO_4 \cdot 2H_2O$), sodium sulfate (Na_2SO_4), absolute ethanol (EtOH), hydrochloric acid (37%) were purchased from Sigma Aldrich. (4-Vinyl-benzyl)-N-methyl-D-glucamine (VbNMG) was properly synthesized in laboratories.

2.2 Synthesis of (4-vinyl-benzyl)-N-methyl-D-glucamine (VbNMG)

The starting monomer was synthesized by suspending NMG (1 g, 5 mmol) in 30 ml of CH_3OH and adding to the suspension an equimolar amount of 4-vinyl-benzyl chloride (0.70 mL, 5 mmol) in presence of Na_2CO_3, according to the reaction reported in **Figure S1**. The reaction mixture was stirred at room temperature monitoring the reaction progress by Thin Layer Chromatography (TLC). Then, the mixture was filtered and the methanol evaporated. The product was purified by crystallization in $CHCl_3$ and characterized by Nuclear Magnetic Resonance an IR spectroscopy (see **Figure S2** and **Figure S3**).

2.3 Synthesis of VbNMG-based polymers by cryopolimerizazion

In a 1.5 mL vial containing 180 µL of H_2O, 40 mg of (4-vinyl-benzyl)-N-methyl-D-glucamine (Vb-NMG) and 3.3 mg of N, N'-methylene-bis-acrylamide (MBAA, molar ratio 1/6 comparing to the moles of monomer) were added. Syntheses of copolymers were performed adding HEMA as co-monomer using the following VbNMG/HEMA molar ratio: 25/75, 50/50, 75/25. HCl 2N was added in small doses to the reaction mixture under vigorous stirring, controlling the pH up to the neutrality (about 50 µL). Additional 24 µL of H_2O was added, then the solution was cooled to 0 °C and 3 µL of a 10% w/v ammonium persulphate (APS) solution in water and 3 µL of a 10% w/v tetramethyl-ethylene-diamine (TEMED) solution in water were added respectively under vigorous stirring. The reaction mixture was stirred for about 1 min and then transferred to a glass micro-reactor with a diameter of about 5.5 mm pre-cooled to 0 °C. The reactor was placed in a cryostat at -14 °C for about 24 hours, then, after thawing, the cryogel obtained was washed with mixtures of H_2O/HCl/EtOH progressively increasing the concentration of EtOH up to pure EtOH. The purified cryogel was dried under nitrogen flow and then under vacuum. The final product consists of a macroporous monolithic cryogel. The yield of reactions ranges from 80 to 85 %.

2.4 Characterizations

All the synthesized materials were accurately characterized. The VbNMG monomer structure was confirmed by ^{1}H and ^{13}C spectra, registered by using Varian "*Mercury 400*" and "*Mercury 600"* spectrometers, operating at 400 and 600 MHz, respectively. TMS was used as a reference.

All formulated samples were characterized by Fourier transform infrared spectroscopy (FTIR) spectroscopy, and the spectra were acquired through a PerkinElmer Spectrum 1000 spectrometer.

Morphologies of the sponges were investigated by scanning electron microscopy (SEM), performed by using a Zeiss Supra 25 field emission microscope. All samples were previously coated with a thin layer of gold (<10 nm) to impart them conductivity.

Samples were subjected to thermogravimetric analyses (TGA) by using a thermogravimetric apparatus (TA Instruments Q500) under nitrogen atmosphere (flow rate 60 mL/min) at 10 °C/min heating rate, from 40 °C to 800 °C. TGA sensitivity is 0.1μg with a weighting precision of ± 0.01%. The isothermal temperature accuracy is ± 1°C.

Swelling tests were performed on dried cylindric samples (4mm×9mm). After water uptake and removal of its surplus from the surface, mass measurements were performed. The total uptake for all samples was determined by calculating the increase of cumulative mass at fixed time intervals. The equilibrium swelling degree was measured weighting the wet sample immersed in water for 30 min, whereas, the adsorption kinetic was estimated after keeping the samples in contact with a slight excess of water for selected times, followed by quick removal of the excess of unabsorbed water. The adsorbed water was evaluated by weight the sample in function of the time, normalizing all data. Swelling−deswelling cycles performance was evaluated on about 20 mg of wet samples. All samples were kept in contact with water and weighted after 5 min of contact time. Then, all samples were squeezed between two paper foils until water residue was removed. After, samples were weighted and kept once more in water to repeat the squeezing procedure up to 5 times. The equilibrium swelling degree can be calculated using the following formula [45].

$$Swelling\ degree = \frac{(m_w - m_d)}{m_d} \qquad \textbf{(1)}$$

where m_w is the weight of the wet cryogel and m_d is the weight of the dry cryogel.

The porosity of the dried sample was determined from eq. (2), by measuring the absorbed volume of cyclohexane versus the total volume of each sample using a pycnometer.

$$Porosity\ \% = \frac{V_{pores}}{V_{sample}} 100 = \frac{m_w - m_d}{m_1 - m_2 + m_w} 100 \qquad \textbf{(2)}$$

where m_d is the mass of dried cryogel, m_w is the mass of the cryogel wet in cyclohexane, m_1 is the mass of the apparatus filled with cyclohexane, m_2 is the mass of the apparatus with cyclohexane plus cryogel [46]. Before each measurement, residual gas entrapped into the cryogel was removed under reduced pressure.

Quantitative determination of metal ions in solution after sequestration procedure was performed by an Inductively Coupled Plasma–Mass Spectrometry (ICP/MS) Nexion 300X (Perkin Elmer Inc. Waltham, Massachusetts, U.S.A.) using the kinetic energy discrimination mode (KED) for interference suppression. Each determination was performed three times. The accuracy of the analytical procedure was confirmed by measuring a standard reference material, Nist 1640a trace element in natural water, without observing an appreciable difference.

Batch equilibrium tests were carried out to calculate the equilibrium retention capacity (Q_e) values as well as the metal ions removal percentage. In general, ~10 mg of cryo-sponges were immersed into either chromium ($K_2Cr_2O_7$) or arsenate ($Na_2HAsO_4 \cdot 7H_2O$) solutions (5 mL and pH=6) at different initial concentration, ranging from 30 to 1400 mg/L (of arsenate or chromium salt). The vials were maintained under constant shaking at 25°C and 180 rpm for 24h, withdrawing aliquots of 100 µL at different intervals time to perform kinetic studies. The residual metal ion concentrations were evaluated by ICP-MS measurements. All experiments were repeated three times reporting a maximum Relative Standard Variation of 5% for As(V) and Cr(VI) and 8% for P(V) . Additionally, to corroborate the obtained results, Atomic Absorption Spectroscopy (AAS) as well as ICP-MS by following the analytical method EPA 30151 2007 + EPA 6020B 2014 were executed in an external laboratory. As expected, all data were nicely reproduced.

For the interfering tests, in order to obtain the final concentrations of 0, 15, 30, 60, 120, 240 and 480 mg/L of sulphate or phosphate salt and 30 mg/L of arsenate or chromium salt, seven different vials containing 500 µL of arsenate salt (60 mg/L) or chromium salt (60 mg/L) solution were mixed with 500 µL of sulphate or phosphate at increasing concentrations (0, 30, 60, 120, 240, 480 and 960 mg/L). In each vial, a weighted sample of cryogel was added and shaken up to 24 h at 25°C and 180 rpm. After that, ICP-MS of As(V), Cr(VI) and P(V) residues was carried out, whereas the contribution of sulphate ions to As(V) or Cr(VI) was extrapolated by difference. To evaluate potential phosphate competition during As(V) or Cr(VI) capture, solutions with 2:1 molar ratio of phosphate salt and arsenate or chromate salts were prepared considering the following concentrations: 480 ppm of phosphate, 300 ppm of arsenate and 250 ppm of bichromate salts.

To study the reusability of VbNMG-100, materials were subjected to six consecutive adsorption/desorption cycles. Specifically, 30 mg/L of arsenate solution was added drop by drop to ~134 mg of sponge to reach the maximum swollen degree. After 5 minutes of contact time, the sponge was squeezed, withdrawing arsenate solution. Then, the sample was kept between two foils of cellulose paper for 10 minutes to remove the excess of arsenate solution before adding the fresh one. The As(V) residue collected after each cycle was measured by ICP-MS.

To evaluate the complete regeneration of cryo-sponge, recycling tests by washing in acidic media the sample were carried out. To this purpose, the material was kept in contact for 24h with 1400 mg/L of arsenate solution. After that, the sponge was regenerated in a column with HCl 1M and washed with water to reach pH=6. The experiment was repeated up to three subsequent cycles. After each cycle both acid and residue arsenate solutions were analysed by ICP-MS.

Three different semi-empirical adsorption kinetic models were used to study and analyze the kinetic performance in As(V) and Cr(VI) adsorption: pseudo-first order, pseudo-second order, and intraparticle diffusion models [47]. Based on the adsorption equilibrium capacity (Qe) calculated by the following equation:

$$\boldsymbol{Q_e = \frac{(C_0 - C_e) \times V}{W}} \qquad \mathbf{(3)}$$

where C_0 (mg/L) is the metal initial concentration, C_e (mg L-1) is the concentration at the equilibrium, V (L) is the volume of water, W (g) is the weight of adsorbent used during the adsorption experiments. Lagergren pseudo-first order model for heterogeneous solid-liquid systems is formulated as follows:

$$\boldsymbol{\ln(Q_e - Q_t) = \ln Q_e - k_1 t} \qquad \mathbf{(4)}$$

where Q_e and Q_t (mg/g) are the amounts of metal ions adsorbed at equilibrium and time t (min), respectively, by using as initial conditions $Q_t = 0$ at t = 0,. The slope value obtained by plotting ln(Q_e-Q_t) versus time (min) (Figure 5(a)), allows estimating the constant rate k_1 (min^{-1}).

Besides eq. (3), the pseudo-second order model allows to calculate the reaction rate k_2 (g $mg^{-1}min^{-1}$), given by the following equation:

$$\boldsymbol{\frac{t}{Q_t} = \frac{1}{k_2 Q_e^2} + \frac{t}{Q_e}} \qquad \mathbf{(5)}$$

By plotting the experimental data t/q versus t, Q_e and k_2 were assessed from the both slope and intercept, respectively (see **Table 1)**.

As well stated, the pseudo-second order equation, better describes the entire metal ions adsorption process than the pseudo-first order model, which is more useful to describe the first 20-30 minutes of the adsorption process [47,48]. On the other hand, eq. (3) can indicate if a chemisorption process occurs taking into account the adsorbent-adsorbate interactions [47].

The intraparticle diffusion model is described with the following equation:

$$\boldsymbol{Q_t = k_i \sqrt{t} + C} \qquad \mathbf{(6)}$$

where k_i is the intraparticle diffusion rate constant (mg $g^{-1}h^{-0.5}$).

To investigate the adsorption equilibrium data for the VbNMG-100 cryo-sponge, Langmuir, Freundlich, Temkin, and Dubinin Radushkevich non-linear models were applied.

Langmuir equation is one of the most important isotherms adsorption model to obtain useful information about the adsorbate/adsorbent interaction and is described by non-linear equation (7) [49, 53]:

$$\mathbf{q_e = \frac{Q_0 b C_e}{1 + b C_e}} \qquad \mathbf{(7)}$$

where q_e (mg g^{-1}) is the content of metal ions adsorbed per unit weight of adsorbate, C_e (mg L^{-1}) is the metal concentration at the equilibrium, Q_0 (mg g^{-1}) is the monolayer capacity and b (mg^{-1} L) represents the constant associated to adsorption heat (K_L). From the K_L parameter it is also possible to calculate the separation factor (R_L) by the below equation (8), useful to describe the efficiency of the adsorption process.

$$\mathbf{R_L = \frac{1}{1 + K_L C_0}} \qquad \mathbf{(8)}$$

where K_L is the Langmuir constant and C_0 corresponds to the adsorbate initial concentration (mg L^{-1}). When the R_L=1 a linear adsorption occurs. R_L>1 is associated with unfavorable adsorption, 0 < R_L < 1 favorable adsorption, and R_L=0 is referred to irreversible adsorption.

The empirical Freundlich sorption model is usually used to describe heterogeneous systems, and thus can be applied to fit the adsorption of As(V) and Cr(VI) onto VbNMG-100 following the linear equation (9) here reported:

$$\mathbf{q_e = K_F (C_e)^{\frac{1}{n_F}}} \qquad \mathbf{(9)}$$

where K_F (mg g^{-1}) is the Freundlich constant associated with the adsorption capacity and $1/n_F$ is a parameter that allows obtaining indications about the heterogeneity of the system, and thus the intensity of the adsorption.

Temkin equation is an isotherm model that takes into account the adsorbate/adsorption interaction on the entire adsorption process. It assumes that the heat of adsorption (ΔH_{ads}) of all interacting molecules linearly decreases by increasing the surface coverage. The linear form of Temkin equation is given by:

$$\mathbf{q_e = B_T \, ln(K_T C_e)} \qquad \mathbf{(10)}$$

where K_T represents the equilibrium binding constant (L mol^{-1}) that corresponds to the maximum binding energy. Whereas, the B_T is a parameter associated to the heat of adsorption and is defined by

$$\mathbf{B_T = \frac{RT}{b_T}} \qquad \mathbf{(11)}$$

with R the ideal gas constant (8.314 J mol^{-1} K^{-1}), T the temperature in Kelvin and b_T defined as the variation of adsorption energy (kJ mol^{-1}).

A more general equation than the Langmuir model is the Dubinin-Radushkevich semiempirical equation in which adsorption follows a pore-filling mechanism. It assumes a multilayer process that involves Van Der Waal's forces, thus indicating the occurrence of a physical adsorption process. As a consequence, by applying the Dubinin-Radushkevich equation it is possible to distinguish between physical and chemical adsorption of metal ions [53, 54]. The linear form of the equation is expressed as follows:

$$\mathbf{q_e} = q_m \, exp\left\{-\beta R^2 T^2 \left[ln\left(1 + \frac{1}{C_e}\right)\right]^2\right\} \quad (12)$$

where β is the Dubinin-Radushkevich constant, R the ideal gas constant (8.314 J mol^{-1} K^{-1}), T is the absolute temperature. From equation 12 it is possible to calculate the Polanyi potential (ε) and the adsorption energy (E_{D-R}) that are given by:

$$\varepsilon = RT \, ln\left(1 + \frac{1}{C_e}\right) \quad (13)$$

$$E_{D-R} = (2\beta)^{-\frac{1}{2}} \quad (14)$$

When E_{D-R} is less than 8 kJ mol^{-1}, typically physisorption occurs. If E_{D-R} consists of a value between 8 and 16 kJ mol^{-1}, the adsorption proceeds by an ion-exchange process. Finally, when E_{D-R} is higher than 16 kJ mol^{-1}, the adsorption is associated to a chemisorption process [53].

3. Results and Discussion

3.1 Cryogels synthesis and characterization

High-quality chelating polymeric materials for water remediation should be designed considering several factors including high surface area and pore size, mechanical and chemical stabilities, high and fast adsorption efficiency. Their recyclability as well as environmental sustainability, are also required. In this work, sponges based on VbNMG at different percentages of HEMA (from 0 to 75%) were synthesized *via* cryostructuration method in water at temperatures below its freezing point (see **Figure 1**). In this way, the formation of 3D stable network occurs around the ice crystals that act as a porogen. The followed thawing generates pores with forms and dimensions depending on the operational parameters used. Therefore, the resulted high porosity of cryogels consists of interconnected micro-, meso- or macro-pores that imply excellent water uptake and fast diffusion. If compared with traditional chelating polymeric systems, cryogels present a much smaller surface area, that for dense samples does not exceed 30 m^2/g [46]. Nevertheless, their high permeability as well

as the peculiar porosity structure provide outstanding accessibility to the chelating sites, maintaining also low back pressure when used as a filter.

The synthesized samples were named depending on the VbNMG percentage content as VbNMG-100, VbNMG-75, VbNMG-50, and VbNMG-25 (for example, VbNMG-25 refers to the sample with 25% Vb-NMG and 75% HEMA). All prepared cryo-sponges were subjected to spectroscopical (see FT-IR in supporting information), morphological and thermal characterizations as well as porosity and swelling tests as reported as follows.

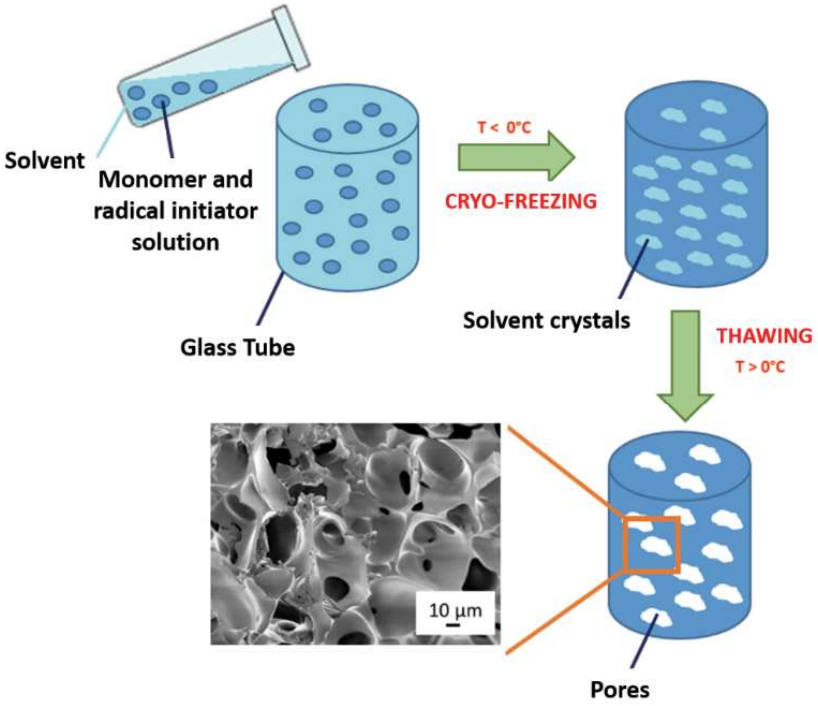

Figure 1. Schematic diagram of VbNMG cryogels synthetic procedure.

3.2 SEM Analyses

The morphology of the VbNMG-100 and related copolymers was studied by scanning electron microscopy (SEM), **Figure 2 (a-d)**. As expected, all cryogels showed a typical macroporous structure. In particular, VbNMG-100 cryogel is characterized by a uniform and regular pore distribution ranging from 20 to 30 µm [see **Figure 2 (a)**]. Differently, moving on VbNMG-75, VbNMG-50 and VbNMG-25, the presence of HEMA monomer induced modification of the porous structure [see **Figures 2(b), (c) and (d)**]. Indeed, by inspection of the high-magnification images [see insets of **Figures 2 (a)-(d)]** of the copolymer sponges**,** a more jagged porous structure and smaller pore size distribution is evidenced. Based on the obtained results, it is expected that the higher pore size distribution identified for VbNMG-100 can positively influence the fast diffusion of water into the interconnected system, by exposing a higher number of NMG active sites in a short time.

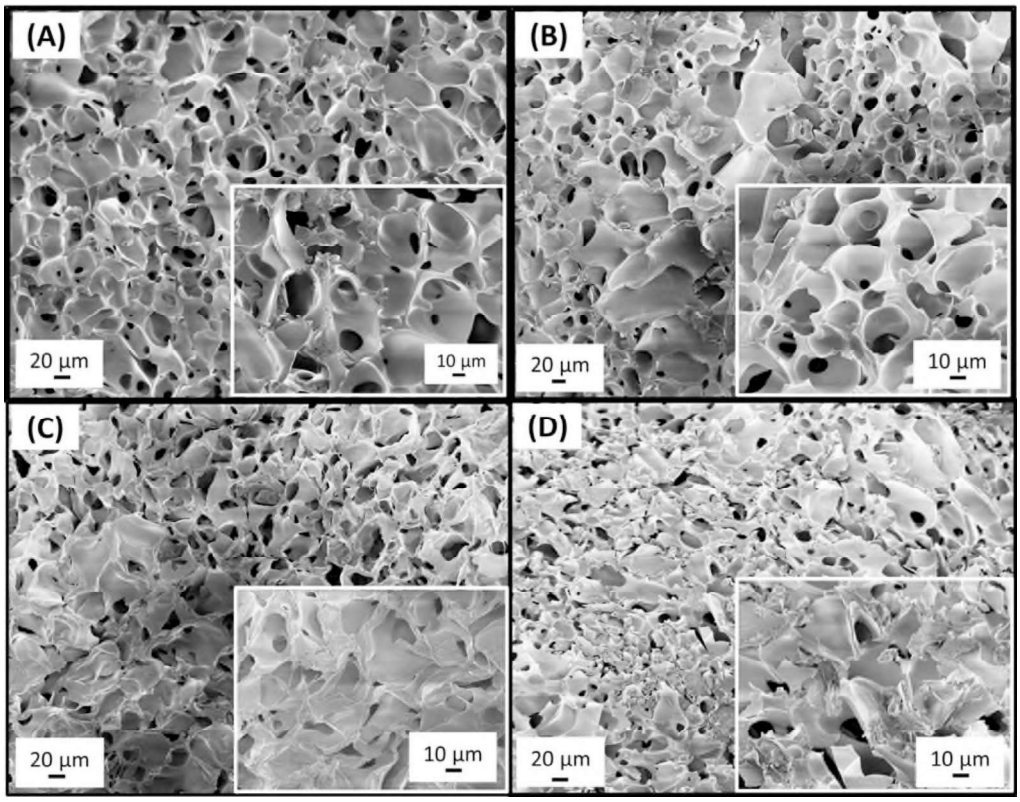

Figure 2. SEM images of **(a)** VbNMG-100, **(b)** VbNMG-75, **(c)** VbNMG-50 and **(d)** VbNMG-25.

3.3 Thermogravimetric analyses (TGA)

Figure 3 (a-b) shows the TGA and DTGA profiles of (4-vinyl-benzyl)-N-methyl-D-glucamine and related copolymers containing 25, 50, and 75% of HEMA. All samples undergo two separate thermal degradation steps beginning from ~200°C up to ~500°C. In agreement with the literature [40], the first thermal degradation step can derive from the decomposition of glucamine chelating groups, whose temperatures at a maximum rate of decomposition (TMD) decreased with increasing of HEMA content. At higher temperatures, the thermal degradation of the poly 4-vinyl-benzyl chain, as well as HEMA moieties, took place, giving TMD in the range of 412 - 425 °C (see **Table S2**). As expected, the residue increased as a function of the aromatic content due to the formation of char.

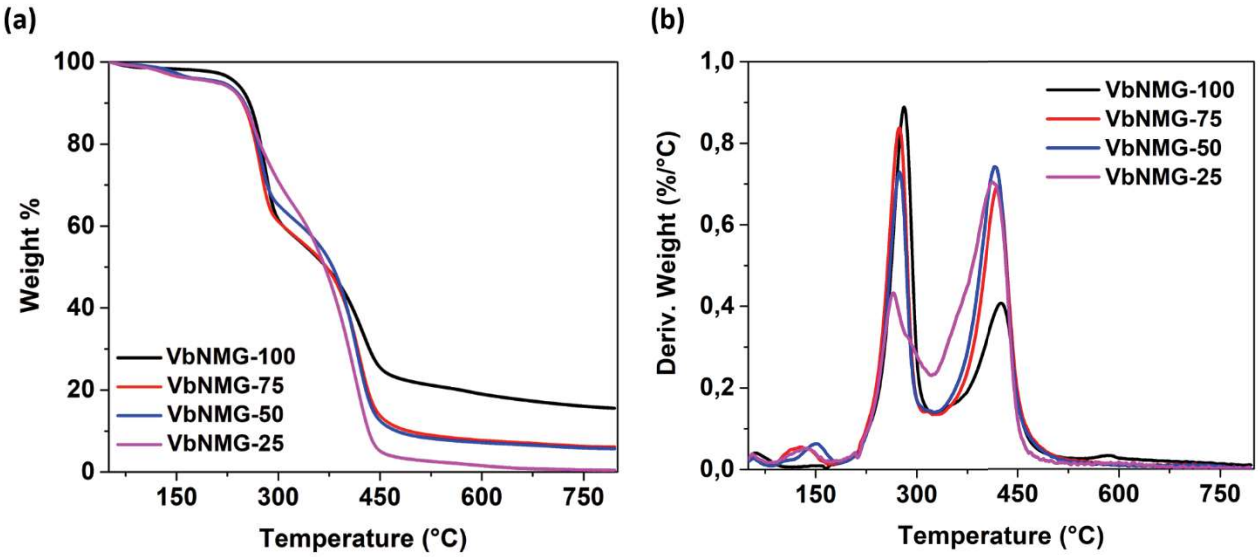

Figure 3. (a) TGA and (**b)** DTGA profiles of VbNMG-100 (black line), VbNMG-75 (red line), VbNMG-50 (blue line), and VbNMG-25 (purple line).

3.4 Porosity and swelling degree tests

The porosity of all synthesized cryogels was measured. Specifically, the porosity values were calculated following the equation (2) reported in the experimental section. The obtained data reported in **Figure S5** evidenced that the porosity of VbNMG materials was not significantly affected by the addition of increasing amounts of HEMA co-monomer. Additionally, to assess that the fabricated materials can work as sponges, absorbing water in a fast way to release it by squeezing, swelling degree measurements were performed. In **Figure 4 (a-b)** the equilibrium swelling degree (ESD) tests, as well as swelling/deswelling degree cycles, were reported. The column bars of **Figure 4 (a)** showed that ESD values follows the order VbNMG-100 > VbNMG-75 ≃ VbNMG-50 > VbNMG-25, with ESD values included in the range 18,2±0,9 and 15,8±1,4 g/g. This finding is in agreement with the increment of VbNMG-100 hydrophilicity since it contains higher number of NMG units. Nevertheless, although VbNMG copolymers exhibited lower water uptake, all samples reached in only two minutes the maximum swelling degree, preserving almost constant the swelling/deswelling ability up to 5 cycles [see **Figure 4 (b)**].

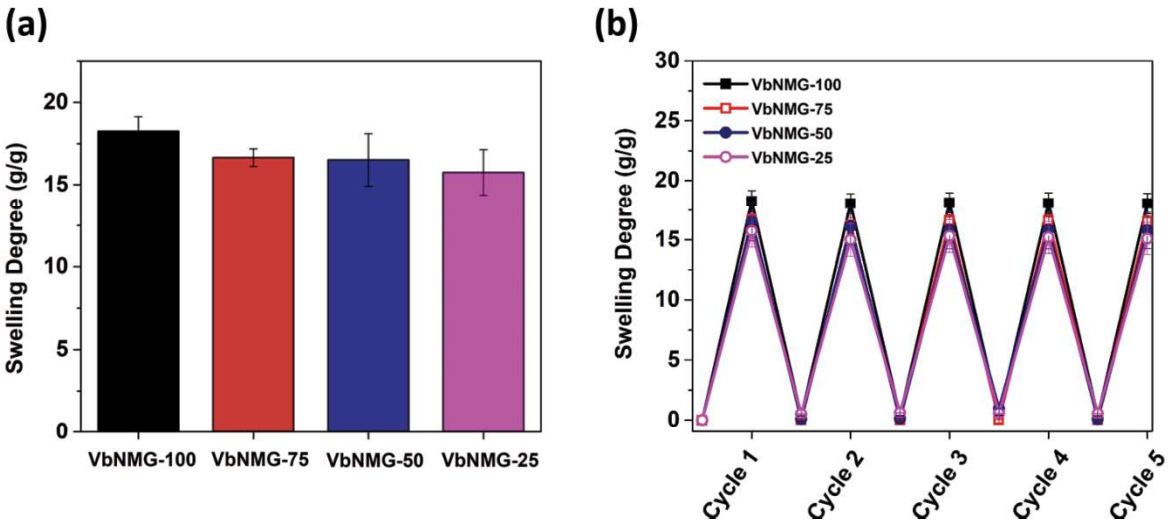

Figure 4. (a) Equilibrium swelling degree and **(b**) Swelling/deswelling cycles of VbNMG samples.

3.5 As(V) and Cr(VI) adsorption studies

Preliminary tests to evaluate the adsorption ability versus As(V) and Cr(VI) of the cryogels depending on their HEMA content were carried out. In particular, metal ions solutions with a 45 ppb concentration were tested by using ~ 8 mg of sample. As it is possible to appreciate from **Table S1**, all VbNMG-based materials were able to reduce the As as well as Cr concentration below 10 µg/L. Specifically, after 8h of contact time, VbNMG-100 showed the best performance with metal ion residues in the water of 1.9 µg/L and 0.7 for As(V) and Cr(VI), respectively. Besides, in view of industrial applications of cryo-sponges in filtering systems and depending on the ion contents to be removed, their sorption capability can be tuned. Indeed, by changing the % of HEMA added during the synthesis it is possible to modulate the sequestrant power assuring also a water swelling aptitude. Based on these excellent results, concentration effect, kinetic profiles studies, interfering ion tests, as well as sorption/desorption capacity of the most performant VbNMG-100 cryogel, were carried out.

3.5.1 Concentration effects

To quantify the capacity of VbNMG-100 cryogel for the removal of As(V) and Cr(VI) from water as a function of the concentration-effect, batch equilibrium procedures were carried out. Six different metal ions solutions were selected with a concentration significantly higher than the permitted WHO limits. No more than 11 mg of cryo-sponge for each batch experiment was used. **Table 1** reports the initial concentrations of metal ion (C_0), the measured concentration at the equilibrium (C_e), the normalized equilibrium capacity (Q_e), and the calculated percentage of metal ion retention after 24h of contact time at room temperature and pH=6.

Table 1. The initial concentration of metal ions (C_0), at the equilibrium (Ce), equilibrium removal capacity (Q_e), and percentage of metal ions removal after 24 h of contact time at room temperature.

As(V)				Cr(VI)			
C_0 (mg L^{-1})	C_e (mg L^{-1})	Q_e (mg g^{-1})	Retention[a] %	C_0 (mg L^{-1})	C_e (mg L^{-1})	Q_e (mg g^{-1})	Retention[a] %
7.7	0.3	4.2	97.6	7.9	0.1	10.2	98.5
17.4	0.5	7.7	97.3	18.1	0.2	18.3	98.9
72.6	1.5	36.5	97.9	68.3	1.3	59.9	98.1
168.4	18.6	69.4	88.9	165.1	10.7	122.5	93.5
338.8	182.5	73.7	46.2	308.1	190.2	125.4	37.1

a $\frac{(C_0 - C_e)}{C_0} \times 100$

As it is possible to see from **Table 1**, all batch experiments showed highly efficient removal of both As(V) and Cr(VI) for all concentration studied, excepted for the highest ones, due to the reaching of cryo-sponge saturation limit.

3.5.2 As(V) and Cr(VI) adsorption kinetic profiles

To determine the adsorption equilibrium time, kinetic profiles were determined [see **Figure 5(a-b)**]. For both metal ions, all experiments were carried out at different initial concentrations and exhibited similar adsorption trends, denoting noteworthy increments for the first 2 hours that level off at 6h, reaching the equilibrium time after about 7h. Furthermore, an increase in the cryogel adsorptive capacity was observed for Cr(VI) if compared to the As(V) removal performance.

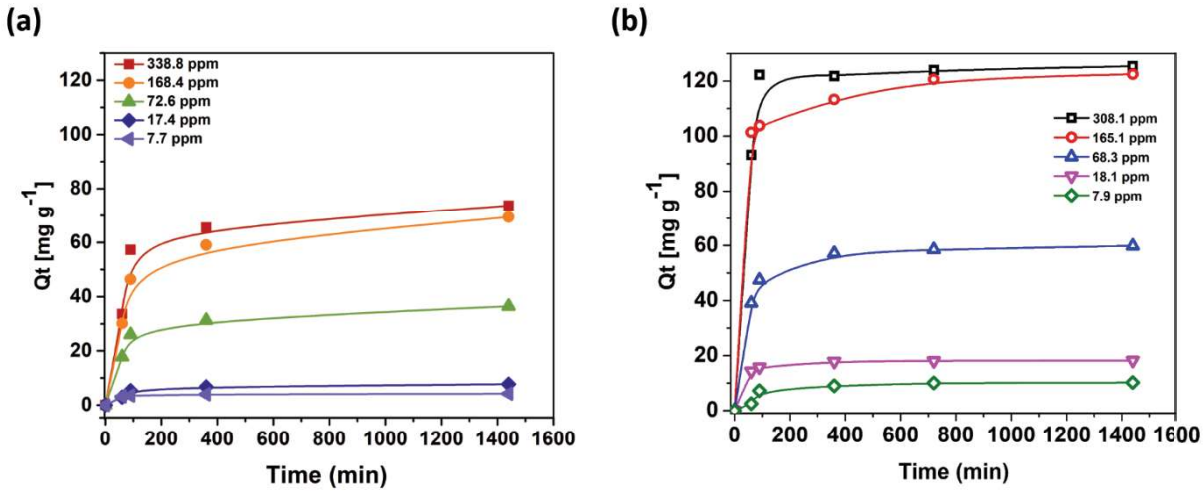

Figure 5. Kinetic profiles of **(a)** As(V) and **(b)** Cr(VI) adsorption calculated for different metal ion concentrations.

From the kinetic point of view, three different models were used (see the experimental section and **Figure S6** and **Figure S7**). In particular, by applying the pseudo-second order model and comparing the extrapolated R-square (R^2), excellent fits for both metal ions were obtained at all tested

concentrations. Further proof of this result was confirmed from the comparison between the theoretical adsorption capacity values (Q_{eT}) with those obtained experimentally (see **Table 2** for both metal ions). Specifically, Q_{eT} derived from equation (5) well matched the experimental values (Q_{exp}), differently to those obtained from equation (4) (see experimental section). The deviance from the linearity of the pseudo-first order model is attributed to an intense initial adsorption process as well as the best fit with the pseudo-second order model allows to assume that the rate-limiting step is the surface adsorption of As(V) and Cr(VI) ions that involve chemisorption [39,50]. According to the literature, at the operating pH (~ 6) the adsorption is controlled by both electrostatic and hydrogen bonding interactions between VbNMG and As(V) and Cr(VI) main anionic forms $H_2AsO_4^-$ /$HCrO_4^-$ [20,31,39,42,51]. Particularly, electrostatic attraction is driven by the protonated tertiary amine, whereas OH groups can promote hydrogen linkages.

As regards the constant rates, it was observed that the K_2 values decreased with increasing initial metal ions concentrations (see **Table 2**). This finding suggested that higher concentrations of metal ions might cause adsorbate surface saturation, in agreement with the lower retention percentage evidenced in the previous section. As a result, a dropping off in the diffusion rate of metal ions occurred. Indeed, deviation from the linearity of the intraparticle diffusion model (see **Table 2**) was also observed [**Figure S6 (c) and Figure S7 (c)**].

Table 2. Kinetic parameters calculated from pseudo-first order, pseudo-second order, and intraparticle diffusion models for As(V) and Cr(VI) adsorption experiments.

	As(V)					Cr(VI)				
C_0	**338.8**	**168.4**	**72.6**	**17.4**	**7.8**	**308.1**	**165.1**	**68.3**	**18.1**	**7.9**
Q_{exp} ($mg\ g^{-1}$)	73.7	69.4	36.5	7.7	4.2	125.4	122.5	59.9	18.3	10.2
	Pseudo I order					**Pseudo I order**				
K_1 x10^{-3} (min^{-1})	5.95	5.04	5.10	5.79	7.18	4.71	4.62	4.76	6.01	5.72
R^2	0.93	0.97	0.93	0.99	0.82	0.43	0.79	0.82	0.81	0.96
Q_{eT} ($mg\ g^{-1}$)	61.72	60.5	30.03	7.11	2.64	29.55	47.90	28.85	6.77	8.42
	Pseudo II order					**Pseudo II order**				
K_2 x10^{-3} (min^{-1})	0.28	0.56	1.55	4.84	25.5	0.85	0.56	0.82	5.35	1.24
R^2	0.99	0.99	0.99	0.99	0.99	0.99	0.99	0.99	0.99	0.99
Q_{eT} ($mg\ g^{-1}$)	75.82	70.37	36.81	7.84	4.2	125.94	123.30	60.57	18.38	10.80
	Intraparticle diffusion					**Intraparticle diffusion**				
R^2	0.57	0.69	0.63	0.66	0.36	0.36	0.41	0.54	0.41	0.69
K_{ip}	1.69	1.63	0.83	0.18	0.09	2.48	2.43	1.31	0.37	0.27

3.5.3 As(V) and Cr(VI) adsorption isotherm models

The Freundlich, Temkin, Dubinin-Radushkevich, and Langmuir isotherm models (see equations 7-14 in the experimental section) were used to investigate the adsorption equilibrium data. From **Figure 6** and the regression coefficient (R^2) reported in **Table 3**, it is possible to deduce that the Langmuir and Dubinin-Radushkevich models are the most suitable to describe both As(V) and Cr(VI) adsorption process onto VbNMG-100 sample. From data fitting, it can also infer that the maximum adsorption capacities (q_m) for As(V) and Cr(VI) were respectively 76.3 and 130.9 (mg g^{-1}) based on Langmuir model. These values are similar to those obtained by using the Dubinin-Radushkevich model. Additional information about the adsorption process can be deduced by calculating the separation factor (R_L) [see equation (8) reported in the experimental section]. Since R_L values were found in the range 0-1 for both metal ions, it can be assumed that the efficiency of the adsorption process is facilitated. Another fundamental parameter that should be taken into account is the mean free energy of adsorption (E_{D-R}) that defines the nature of metal ion/adsorbent interaction (e.g. physical, ion exchange, or chemisorption). As reported in the experimental section, for values lower than E<8 kJ/mol physical adsorption of the arsenate and chromate anion was suggested.

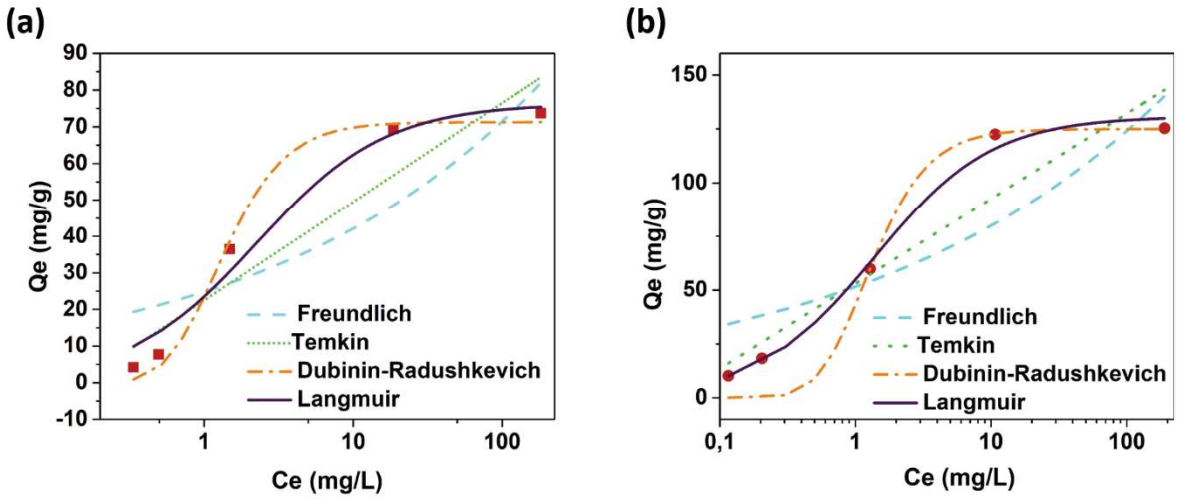

Figure 6. Equilibrium adsorption isotherms by plotting Q_e versus C_e experimental data for **(a)** As(V) and **(b)** Cr(VI) for VbNMG-100 cryogel.

Table 3. Parameters obtained by applying Langmuir, Freundlich, Temkin and Dubinin-Reduschkevic for As(V) and Cr(VI).

	Langmuir				**Freundlich**		
Metal ion	**q_m (mg/g)**	**K_L (L/mg)**	**R_L**	**R^2**	**K_F (mg/g)**	**n_F**	**R^2**
As(V)	76.34	0.45	0.007-0.22	0.97	24.84	4.35	0.77

Cr(VI)	130.9	0.72	0.0045-0.15	0.99	51.55	5.26	0.76
	Temkin				**Dubinin-Radushkevich**		
Metal ion	**B_t (KJ/mol)**	**K_T (L/mg)**	**R^2**		**q_m (mg/g)**	**E_{D-R} (kJ/mol)**	**R^2**
As(V)	11.72	6.83	0.90		71.29	1.16	0.99
Cr(VI)	17.17	21.97	0.89		124.9	1.18	0.96

Among all aforementioned parameters, the Q_m value is considered a useful parameter to compare the adsorption ability of different materials. Therefore, in **Table 4** were also showed the Q_m values of VbNMG-100 and similar NMG-based polymers as well [31,39,41,42,52]. VbNMG-100 exhibited much better performance in terms of Q_m value if compared with the commercial IRA-743, NMG based resins [31,39,41,42]. It is worth noting that results reported by Polowczyk et al., showed an outstanding value of chromium uptake of 677.9 mg/g using a post functionalized resin. However, this result could be ascribed to the more acidic conditions (pH 2-5) that improved the oxyanion chelation, as well as to the grafting of 4-vinylbenzyl trimethylammonium chloride (VbTMA) as additional active sites. On this basis, we will expect a significant improvement by combining cryo-system with the approach used by Polowczyk et al. [35].

Table 4. A comparison of Q_m values of NMG-based polymers reported in the literature with the as-synthesized VbNMG-100 cryogel. All compared data are referred to batch equilibrium experiments tested at similar C_0 performed at pH~6 and room temperature. Definition of the reported acronyms are listed in supporting information.

Year	NMG-based materials	As(V) Q_m (mg g^{-1})	Cr(VI) Q_m (mg g^{-1})	Time of contact	References
2020	VbNMG-100	76.3	130.8	24h	This work
2015	P(VbNMDG-co-ClVBTA)	/	677.9*	24h	[35]
2014	Grafted NMDG membrane	67.1	/	/	[52]
2012	PVbNMDG nanocomposite	55.2	/	48h	[31,39]
2004	NMDG	60.5	/	3d	[41]
2004	IRA 743	14.7	/	3d	[41]
2010	IRA-743	/	29.3	1h	[42]

*the adsorption experiments were executed at pH 4-5

A comparison of VbNMG-100 performance with the most recent and relevant findings concerning the sorption ability of As(V) and Cr(VI) [12,18,19,22,36,53-68] was also reported (see **Table 5**). From a general point of view, VbNMG-100 presents highly competitive ability versus both As(V) and Cr(VI) sorption, although higher values were observed by using other systems. Su et al. proposed

the freeze-drying technique to obtain a three-dimensional oriented honeycomb-like structured iron/chitosan composite, improving the As(V) capture up to 86.9 mg/g. In this case, the sequestration process was significantly enhanced by the presence of nanoscale zero-valent iron particles [18]. However, if not properly attached to the material, the use of nanoparticles for water remediation can cause a serious threat to aquatic and human life. Besides, by looking at the Cr(VI) Q_m values of several adsorbents, it is noteworthy that the operating pH value plays a key role. Depending on the material, more acidic conditions improve the oxyanion chelation [59,60,62,64,65]. Tu et al. reported a Cr(VI) maximum adsorption of 386.1 mg g^{-1} by operating at a pH value of 2. Even if this value is remarkable, it is also important to highlight that in the water purification field, analysis has to be performed in conditions as close as possible to the real ones [59].

Table 5. Comparison of Q_m values of different adsorbent materials reported in the most recent literature with the as-synthesized VbNMG-100 cryogel. All compared data are referred to batch equilibrium experiments tested at similar C_0 performed and room temperature. Definition of the reported acronyms are listed in supporting information.

Year	Adsorbent materials	As(V) Q_m (mg g^{-1})	Cr(VI) Q_m (mg g^{-1})	pH	Time of contact	References
2020	VbNMG-100	76.3	130.8	6	24h	This work
2020	DMAA hydrogel	14.2	/	6	2d	[56]
2020	CZA	42.	/	6	20h	[53]
2020	PVC/PE	11.6	/		40min	[57]
2020	CS-SSM	/	112.5	5	2h	[58]
2020	BGAC	/	386.1	2	18h	[59]
2019	Magnetic Char	19.9	/	6	1h	[60]
2019	PVDF-HFP/PAni	/	15.1	4.5	24h	[61]
2017	F-PANI2	/	171.2	2	200min	[62]
2017	Fe_3O_4@CelHT	/	27.2	6	70min	[63]
2016	nZVI/chitosan	86.9	/	6	24h	[18]
2016	TiO_2	3.1	/	3	4h	[64]
2015	AMGO	/	123.4	2	12h	[65]
2015	Ni/Ni_xB-NPCR	17.8	/	6	22h	[66]
2014	Activated carbon	17.9	/	6	24h	[67]
2014	GC composite beads	54.8	/	7.5	10h	[68]

3.5.4 Interfering Tests

It was demonstrated that the chelating effect showed by NMG is mainly driven by the protonated amine that forms electrostatic interactions with oxyanion groups such as borate, arsenate, phosphate, sulfate, and chromate [69]. An important role is also played by the hydroxyl groups in performing the complexation of oxyanions by forming monochelates and/or bischelates complexes [70]. As shown

in Figure 7, these oxyanions possess structural similarities. Therefore, when simultaneously present in solution, they can compete with each other to form NMG complexes. Particularly, arsenate is comparable to phosphate in terms of electrochemical properties, size, and degree of polarization, determining an analogous behaviour in diffusion and adsorption. Nevertheless, some parameters such as pH, concentration, charge, and ion strength of the solution, can regulate their preferential adsorption to the material surface [71].

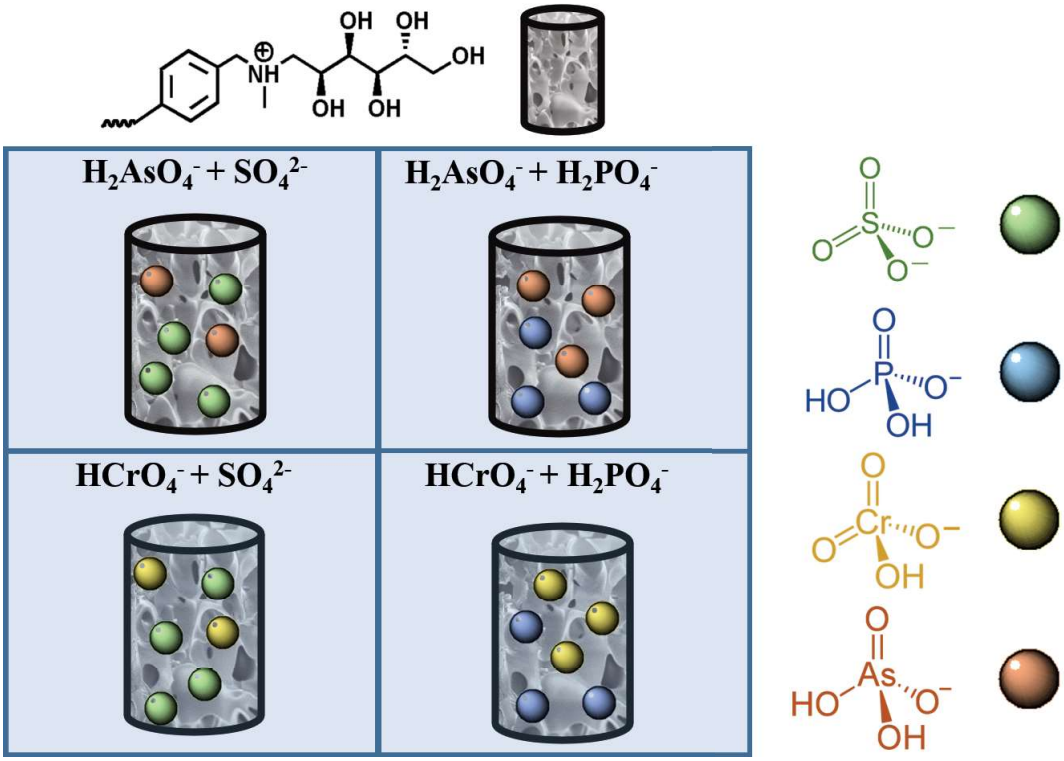

Figure 7. Schematic representation of sulphate and phosphate interference during As(V) and Cr(VI) adsorption process

In agreement with the main factor that governs the adsorption process for NMG resins, the order in interfering As(V) retention is trivalent ions > divalent ions >monovalent ions [69]. Specifically, sulphate ions having a double charge, interact more strongly with the amine sites reducing its ability in attracting the monocharged arsenate. Similarly, chromate anions being mainly monocharged at pH 6, should result weaker than sulphate in binding NMG functional group **(Figure 7).** Considering data reported in the literature [39,41,53,70-72], we are confident in assuming that also NMG cryogel presents a high affinity for all aforementioned species. As well, it is reasonable to suppose that the macroporous structure allowed equal accessibility to the chelating sites for all of them. Consequently, at fixed pH, NMG/oxyanions complexation should mainly depend on the number of available sites and ions charge as well.

In light of this, the interference of sulphate and phosphate was studied (see **Figure 8a-b**), by increasing their concentration from 0 to 480 mg/L at a fixed arsenate or chromate content. These selected values are much higher than those imposed for drinking water [7]. At the same time, surface saturation effects, that can restrain the diffusion of ions into the material, have to be avoided during the experiment.

In **Figure 8 (a-b)** it is possible to observe that the presence of phosphate did not affect the As (V) and Cr(VI) sorption process of the cryogel for all oxyanion concentration tested, maintaining high sorption retention (~99%). Conversely, both As(V) and Cr(VI) retention were influenced by the presence of sulphate ions. In particular, by adding concentration higher than 60 mg/L, As(V) as well as Cr(VI) uptake was significantly reduced from 98% to 12.3 % and from 98% to 26%, respectively. As expected, the role of sulphate was clear cut, and in excellent agreement with the literature as well [19, 31, 34, 39].

From the same set of experiments, it is possible to achieve simultaneously values of P(V) sorption. In **Table S3** and **Table S4** P(V) uptake values obtained from the same solutions were reported. From data collected, it was evident that NMG cryogel can efficiently remove phosphate ions if concomitant present in solution. Given that, it is likely to suppose that the cryogel presents free chelating sites, able to adsorb both ions with the same efficiency. However, to obtain more information on preferential adsorption of arsenate or chromate versus phosphate ions, solutions containing 1:2 molar ratio of arsenate or chromate versus phosphate ions were prepared (see experimental part). After 24h of cryogel/solution contact time, ICP-MS measurements evidenced an As(V) removal of 96% and 75% for phosphorus P(V). Similarly, 98% of Cr(VI) and 77% of P(V) uptake were detected. These data might suggest slightly preferential adsorption of As(V) and Cr(VI) in the presence of P(V) interfering ions. Even if it was demonstrated that phosphate ions are more susceptible to pH and ion strength variation compared to arsenate [72], such kind of studies certainly required further and specific investigations. To further corroborate the ability of VbNMG-100 in sequestering selected species, a mixed solution composed by 30 mg/L of phosphate, 30 mg/L of sulphate and 30 mg/L of As(V) or Cr(VI) (**Figure S8**) was kept in contact with the sponge for 24h. In this experiment, values registered for As(V) and P(V) uptakes were 98.8% and 92.4 % respectively. Similarly, in the presence of chromate ions, the % of removal was 98.8 for Cr(VI) and 89.9 for P(V), which nicely confirmed interfering tests discussed before in **Figure 8(a-b)**.

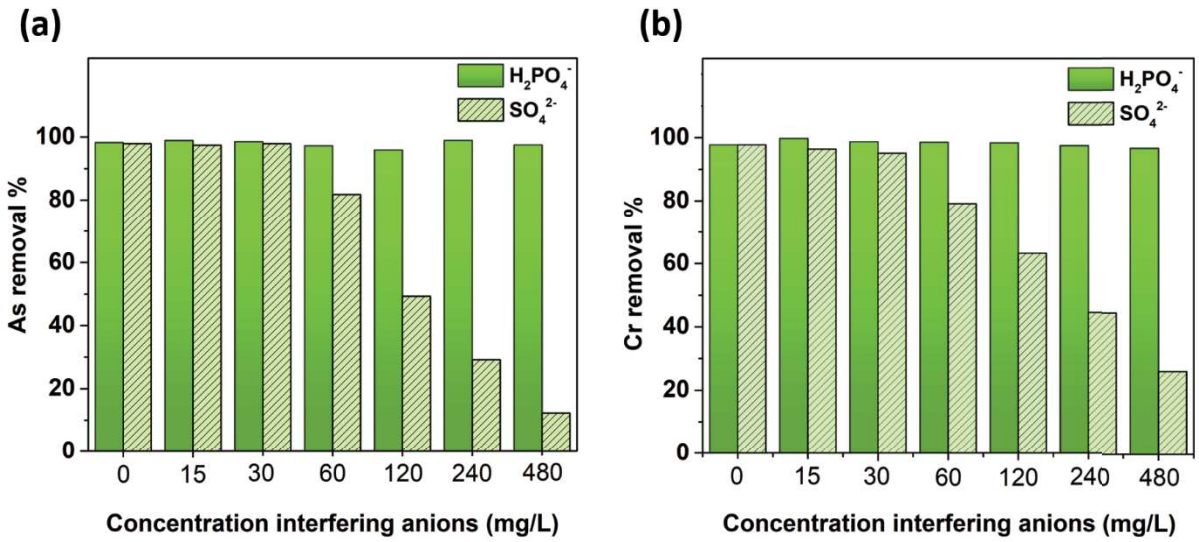

Figure 8. Effect of phosphate (green bar) and sulphate (green medium bar) oxyanions on **(a)** As(V) adsorption and **(b)** Cr(VI) [oxyanions dosage: 0-480 mg/L, As(V) and Cr(VI) solution: 30 mg/L].

3.5.5 Sorption/desorption and regeneration cycles

To evaluate the adsorbent lifetime, adsorption/desorption experiments were carried up to 6 subsequent cycles. Specifically, VbNMG-100 cryo-sponge was swelled by using an As(V) solution, removing it after 5 minutes of contact time by squeezing. The concentration of the as-recovered As(V) solution was quantified by ICP-MS [see **Figure 9 (a)-(b)**]. In particular, as it is possible to observe in **Figure 9(b)**, up to 6 subsequent sorption/desorption steps, the adsorption efficiency of VbNMG-100 was maintained for all tested cycles.

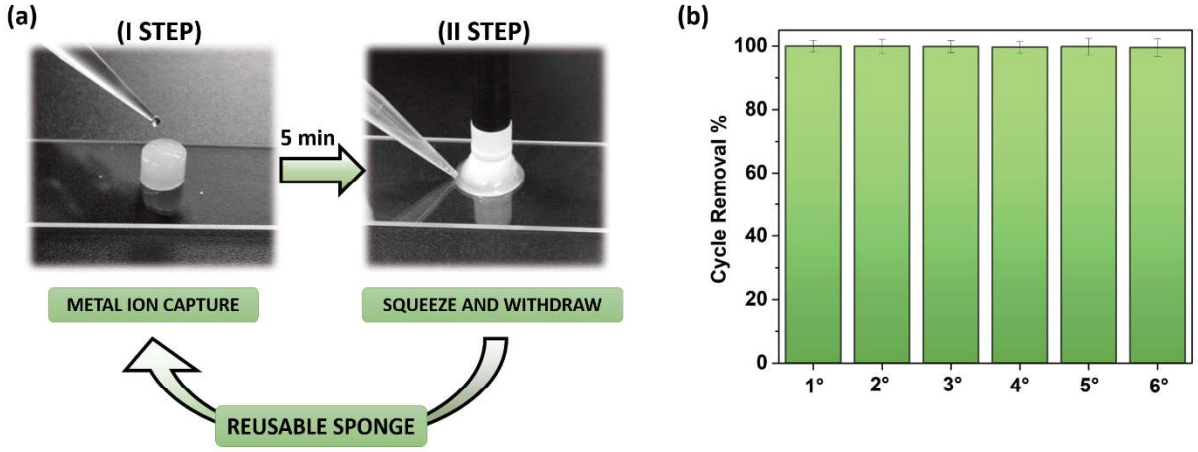

Figure 9. (a) Scheme of the purification process repeated up to 6 cycles. After 5 minutes of contact time, the arsenate solution (30 mg/L) was removed by a simple cryogel squeezing. **(b)** ICP-MS of the withdrawn As(V) solutions showed removal of ~99% up to 6 repeated cycles.

Based on these outstanding results, we also assessed the regeneration ability of the sponge after the sorption/desorption test. To this purpose, after the last squeezing process, VbNMG-100 was regenerated by HCl solution (see experimental section), calculating the As(V) concentration of the eluted solution [see **Figure S9(a)**]. Then, the regenerated sponge was used again to the sorption/desorption test as described above. VbNMG-100 was subjected up to three regeneration steps. The corresponding Q_e values reported in **Figure S9(b)** demonstrated the efficient reusability of the regenerated sponge for all tested cycles. Thus, these results can be considered a further proof of the excellent performance of VbNMG-100 in sorption/elution cycles.

4. Conclusions

An innovative and sustainable macroporous hydrogel based on NMG, able to eliminate As(V) and Cr(VI) from water has been proposed. Hydrophilic sponges fabricated by cryo-structuration in water showed outstanding sequestrant activity versus both metal ions even present in low concentrations. Specifically, VbNMG-100 sorption was well described by the Langmuir isotherm, exhibiting 76.3 mg/g in arsenic removal whereas chromium is assessed to 130.9 mg/g. With regards the sorption kinetics the best fit was found by applying the pseudo-second order model allows to assume that the rate-limiting step is the surface adsorption of As(V) and Cr(VI) ions that involve chemisorption. If compared with other similar NMG-based formulates, VbNMG-100 offered superior sequestering performances. This peculiar property is reasonably ascribed to the macroporous nature that provides a water fast-diffusion pathway, determining exhaustive access to the chelating sites boosting the ions sequestration. Furthermore, *via* a simple squeeze process (after absorption of polluted water), it is possible to withdraw purified water in only 5 min of contact time, obtaining the 99% of As(V) ion capture for each cycle up to 6 times. To close the loop, its regeneration was achieved by facile acid treatment, restoring the initial chelating properties. Up to three recycling, the sponge can be reused as described, maintaining its performance. Owing to the outstanding results obtained also in terms of sustainable preparation, the present paper is part of an applied patent (application number: 102019000012339).

Acknowledgments

The authors thank the anonymous reviewers for their constructive comments.

References

[1] M. M. Mekonnen, A. Y. Hoekstra, 2016. Four billion people facing severe water scarcity. Sci. Adv. 2, e1500323;

[2] S. Bolisetty, M. Peydayesh, R. Mezzenga, Sustainable technologies for water purification from heavy metals: review and analysis, Chem. Soc. Rev. 48 (2019) 463-487;

[3] P. B Tchounwou, C.t G Yedjou, A. K Patlolla, D. J Sutton, Heavy Metals Toxicity and the Environment, NIH Public Access 101 (2012) 133–164;

[4] J. H. Duffus, "Heavy metals" a meaningless term?(IUPAC Technical Report), Pure and applied chemistry, 74(5) (2002) 793-807;

[5] H. Bradl, (Ed.), Heavy metals in the environment: origin, interaction and remediation, Elsevier, 2005;

[6] D. K. Gupta, S. Tiwari, B.H.N. Razafindrabe, S. Chatterjee, Arsenic Contamination from Historical Aspects to the Present, in: D.K. Gupta, S. Chatterjee (Eds.), Arsenic Contamination in the Environment, Springer, Cham, 2017, pp 1-12.

[7] World Health Organization (WHO), Drinking Water Parameter Cooperation Project: Support to the revision of Annex I Council Directive 98/83/EC on the Quality of Water Intended for Human Consumption (Drinking Water Directive), WHO: Geneva, Switzerland, 2017;

[8] S. Chowdhury, M. J. Mazumder, O. Al-Attas, T. Husain, Heavy metals in drinking water: occurrences, implications, and future needs in developing countries, Sci. Total Environ. 569 (2016) 476-488;

[9] Y. Salameh, A. B. Albadarin, S. Allen, G. Walker, M.N.M. Ahmad, Arsenic (III, V) adsorption onto charred dolomite: charring optimization and batch studies, Chem. Eng. J. 259 (2015) 663-671;

[10] C. F. Carolin, P. S. Kumar, A. Saravanan, G. J. Joshiba, M. Naushad, Efficient techniques for the removal of toxic heavy metals from aquatic environment: A review., J. Environ. Chem. Eng. 5(3) (2017) 2782-2799;

[11] Y. Huang, X. Feng, Polymer-enhanced ultrafiltration: Fundamentals, applications and recent developments, J. Memb. Sci. 586 (2019) 53–83;

[12] Y. Deng, Q. Zhang, Q. Zhang, Y. Zhong, P. Peng, Arsenate removal from underground water by polystyrene-confined hydrated ferric oxide (HFO) nanoparticles: effect of humic acid, Environ. Sci. Pollut. Res. 27 (2020) 6861–6871;

[13] T. V. Nguyen, S. Vigneswaran, H. H. Ngo, J. Kandasamy, Arsenic removal by iron oxide coated sponge: Experimental performance and mathematical models, J. Hazard. Mater. 182 (2010) 723–729;

[14] S. R. Chowdhury, E. K. Yanful, Arsenic and chromium removal by mixed magnetite-maghemite nanoparticles and the effect of phosphate on removal, J. Environ. Manage. 91 (2010) 2238-2247;

[15] S. Pathan, S. Bose, Arsenic Removal Using “Green” Renewable Feedstock-Based Hydrogels: Current and Future Perspectives, ACS Omega 3 (2018) 5910−5917;

[16] S. Anjum, D. Gautam, B. Gupta, S. Ikram, Arsenic Removal from Water: An Overview of Recent Technologies, The IUP Journal of Chemistry 2 (3) (2009) 7-52;

[17] Q. Wu, M. Liu, X. Wang, A novel chitosan based adsorbent for boron separation, Sep. Purif. Technol. 211 (2019) 162–169;

[18] F. Su, H. Zhou, Y. Zhang, G. Wang, Three-dimensional honeycomb-like structured zero-valent iron/chitosan composite foams for effective removal of inorganic arsenic in water, J. Colloid Interfac. Sci. 478 (2016) 421–429;

[19] B. Moraga, L. Toledo, L. Jelínek, J. Yanez, B. L. Rivas, B. F. Urbano, Copolymer- hydrous zirconium oxide hybrid microspheres for arsenic sorption, Water Research. 166 (2019) 115044;

[20] I. Savina, N., G. C. Ingavle, A. B. Cundy, S. V. Mikhalovsky, A simple method for the production of large volume 3D macroporous hydrogels for advanced biotechnological, medical and environmental applications. Sci. Rep., 6 (2016) 21154;

[21] A. Dąbrowski, Adsorption—from theory to practice, Adv. Colloid. Interfac. 93(1-3) (2001) 135-224;

[22] J. Jachuła, Z. Hubicki, Removal of Cr(VI) and As(V) ions from aqueous solutions by polyacrylate and polystyrene anion exchange resins, Appl. Water Sci. 3 (2013) 653–664;

[23] I. Ali, V. K. Gupta, Advances in water treatment by adsorption technology, Nat. Protoc., 1(6) (2006) 2661;

[24] D.B. Singh, G. Prasad, D.C. Rupainwar, Adsorption technique for the treatment of As(V)-rich effluents, Colloids Surfaces A: Physicochem. Eng. Aspects 111 (1-2) (1996) 49-56;

[25] N. Ricci Nicomel, K. Leus, K. Folens, P. Van Der Voort, G. Du Laing 1, Review Technologies for Arsenic Removal from Water: Current Status and Future Perspectives, Int. J. Environ. Res. Public Health 13 (2016) 62;

[26] D. Mohana, C. U. Pittman Jr, Arsenic removal from water/wastewater using adsorbents—A critical review, J. Hazard. Mater. 142 (1-2) (2007) 1–53;

[27] M. Ussia, A. Di Mauro, T. Mecca, F. Cunsolo, G. Nicotra, C. Spinella, P. Cerruti, G. Impellizzeri, V. Privitera, S. C. Carroccio, ZnO–pHEMA Nanocomposites: An Ecofriendly and Reusable Material for Water Remediation, ACS Appl. Mater. Inter. 10 (46) (2018) 40100-40110;

[28] H. Wang, X. Ji, M. Ahmed, F. Huang, J. L. Sessler, Hydrogels for anion removal from water, J. Mater. Chem. A 7 (2019) 1394;

[29] S. C. Tang, D. Y. Yan, I. M. Lo, Sustainable wastewater treatment using microsized magnetic hydrogel with magnetic separation technology, Ind. Eng. Chem. Res. 53 (40) (2014) 15718-15724;

[30] S. Chatterjee, M. W. Lee, S. H. Woo, Adsorption of congo red by chitosan hydrogel beads impregnated with carbon nanotubes, Bioresource technol. 101 (6) (2010) 1800-1806;

[31] B F. Urbano, B. L. Rivas , F. Martinez , S. D. Alexandratos, Water-insoluble polymer–clay nanocomposite ion exchange resin based on N-methyl-D-glucamine ligand groups for arsenic removal, React. Functi. Polym. 72 (2012) 642–649;

[32] U. Schilde, H. Kraudelt, E. Uhlemann, Separation of the oxoanions of germanium, tin, arsenic, antimony, tellurium, molybdenum and tungsten with a special chelating resin containing methylaminoglucitol groups, React. Polym. 22 (1994) 101-106;

[33] I. Polowczyk , P. Cyganowski , B.F. Urbano , B. L. Rivas ,M. Bryjak, N. Kabay, Amberlite IRA-400 and IRA-743 chelating resins for the sorption and recovery of molybdenum(VI) and vanadium(V): Equilibrium and kinetic studies, Hydrometallurgy 169 (2017) 496–507;

[34] G. Ozkula, B. F. Urbano, B. L. Rivas, N. Kabayc, M. Bryjak, Arsenic Sorption using mixtures on ion exchange resins containing N- Methyl-D-glucamine and quaternary ammonium groups, J. Chil. Chem. Soc., 61 (1) (2016) 2752-2756;

[35] I. Polowczyk, B. F. Urbano, B. L. Rivas, M. Bryjak, N. Kabay, Equilibrium and kinetic study of chromium sorption on resins with quaternary ammonium and N-methyl-D-glucamine groups, Chem. Eng. J. 284 (2016) 395–404;

[36] B. L. Rivas, J. Sánchez, Soluble polymer containing an N-methyl-D-glucamine ligand for the removal of pollutant oxy-anions from water, ACS In Stereochemistry and Global Connectivity: The Legacy of Ernest L. Eliel Volume 1 (2017) 197-211;

[37] P. Santander , B.L. Rivas, B. Urbano, L. Leiton, I. Y. Ipek , M. Yuksel, N. Kabay, M. Bryjak, Removal of Cr(VI) by a chelating resin containing N-methyl-D-glucamine, Polym. Bull. 71 (2014) 1813–1825;

[38] L. Toledo, B. L. Rivas, B. F. Urbano, J. Sánchez, Novel N-methyl-D-glucamine-based water-soluble polymer and its potential application in the removal of arsenic, Sep. Purif. Technol. 103 (2013) 1–7;

[39] B. F. Urbano, B. L. Rivas ,F. Martinez, S. D. Alexandratos, Equilibrium and kinetic study of arsenic sorption by water-insoluble nanocomposite resin of poly[N-(4-vinylbenzyl)-N-methyl-D-glucamine]-montmorillonite, Chem. Eng. J. 193 (2012) 21–30;

[40] T. M. Ting, M. M. Nasef, K. Hashimb, Tuning N-methyl-D-glucamine density in a new radiation grafted poly(vinyl benzyl chloride)/nylon-6 fibrous boron-selective adsorbent using the response surface method, RSC Adv. 5 (2015) 37869;

[41] L. Dambies, R. Salinaro, S. D. Alexandratos, Immobilized N-Methyl-D-glucamine as an arsenate-selective resin, Environ. Sci. Technol. 38 (2004) 6139-6146;

[42] M. R. Gandhi, N. Viswanathan, S. Meenakshia, Adsorption mechanism of hexavalent chromium removal using Amberlite IRA 743 resin, Ion Exch. Lett. 3 (2010) 25-35;

[43] S. Sayin, F. Ozcan, M. Yilmaz, Synthesis and evaluation of chromate and arsenate anions extraction ability of a N-methylglucamine derivative of calix[4]arene immobilized onto magnetic nanoparticles, J. Hazard. Mater. 178 (2010) 312–319;

[44] M. M. Nasef, T.M. Ting A. Abbasi, A. Layeghi-moghaddam, S. S. Alinezhad, K. Hashim, Radiation grafted adsorbents for newly emerging environmental applications, Radiat. Phys. Chem. 118 (2016) 55–60;

[45] D. C. Wang, H. Y. Yu, M. L. Song, R. T. Yang, J. M. Yao, Superfast adsorption–disinfection cryogels decorated with cellulose nanocrystal/zinc oxide nanorod clusters for water-purifying microdevices, ACS Sustain. Chem. Eng. 5 (8) (2017) 6776-6785;

[46] O. Okay (Ed.), Polymeric Cryogels: Macroporous gels with remarkable properties, Vol. 263, Springer, 2014;

[47] A. Bonilla-Petriciolet, D. I. Mendoza-Castillo, H. E. Reynel-Ávila, (Eds.), Adsorption processes for water treatment and purification, Netherlands: Springer, 2017;

[48] Y. S. Ho, Review of second-order models for adsorption systems. J. Hazard. Mater. 136 (3) (2006) 681-689;

[49] G. Alberti, V. Amendola, M. Pesavento, R. Biesuz, Beyond the synthesis of novel solid phases: review on modelling of sorption phenomena, Coord. Chem. Rev. 256 (1-2) (2012) 28-45;

[50] D. Robati, Pseudo-second-order kinetic equations for modeling adsorption systems for removal of lead ions using multi-walled carbon nanotube, J. Nanostructure Chem. 3 (1) (2013) 55;

[51] J. A. R. Guivar, A. Bustamante, J. C. Gonzalez, E. A. Sanches, M. A. Morales, J. M. Raez, M. J. L. Muñoz, A. Arencibia, Adsorption of arsenite and arsenate on binary and ternary magnetic nanocomposites with high iron oxide content, Appl. Surf. Sci. 454 (2018) 87-100;

[52] N. R. Shinde, V. Chavan, R. Acharya, N.S. Rajurkar, A.K. Pandey, Selective removal of arsenic(V) from natural water using N-methyl-Dglucamine functionalized poly(propylene) membranes, J. Env. Chem. Eng. 2 (2014) 2221-2228;

[53] H. Bessaies, S. Iftekhar, B. Doshi, J. Kheriji, M. C. Ncibi, V. Srivastava, M. Sillanpää, B. Hamrouni, Synthesis of novel adsorbent by intercalation of biopolymer in LDH for the removal of arsenic from synthetic and natural water, J. Environ. Sci. 91 (2020) 246-261;

[54] N. Ayawei, A. N. Ebelegi, D. Wankasi, Modelling and interpretation of adsorption isotherms, J. Chem-NY, (2017) 2017;

[55] D. V. Morales, B.L. Rivas, N. Escalona, Poly([(2-methacryloyloxy)ethyl]trimethylammonium chloride): synthesis, characterization, and removal properties of As(V), Polym. Bull. 73 (2016) 875–890;

[56] H. Tokuyama, E. Kitamura, Y. Seida, Development of zirconia nanoparticle-loaded hydrogel for arsenic adsorption and sensing, Reactive and Functional Polymers 146 (2020) 104427;

[57] E. Singh, A. Kumar, A. Khapre, P. Saikia, S.K. Shukla, S. Kumar, Efficient removal of arsenic using plastic waste char: Prevailing mechanism and sorption performance, J. Wat. Proc. Eng. 33 (2020) 101095;

[58] A.M. Abdel-Mohsen, J. Jancar, L. Kalina, A.F. Hassan, Comparative study of chitosan and silk fibroin staple microfibers on removal of chromium (VI): Fabrication, kinetics and thermodynamic studies, Carbohydrate Polymers 234 (2020) 115861;

[59] B. Tu, R. Wen, K. Wang, Y. Cheng, Y. Deng, W. Cao, K. Zhang, H. Tao, Efficient removal of aqueous hexavalent chromium by activated carbon derived from Bermuda grass, J. Colloid Interfac. Sci. 560 (2020) 649-658;

[60] A. Zubrik, M. Matik, M. Lovás, Z. Danková, M. Kaňuchová, S. Hredzák, J. Briančin, V. Šepelák, Mechanochemically Synthesised Coal-Based Magnetic Carbon Composites for Removing As (V) and Cd (II) from Aqueous Solutions, Nanomaterials 9 (1) (2019) 100;

[61] G. Dognani, P. Hadi, H. Ma, F.C. Cabrera, A.E. Job, D.L. Agostini, B.S. Hsiao, Effective chromium removal from water by polyaniline-coated electrospun adsorbent membrane, Chem. Eng. J. 372 (2019) 341-351;

[62] S. Das, P. Chakraborty, R. Ghosh, S. Paul, S. Mondal, A. Panja, A.K. Nandi, Folic acid-polyaniline hybrid hydrogel for adsorption/reduction of chromium (VI) and selective adsorption of anionic dye from water, ACS Sust. Chem. Eng. 5(10) (2017) 9325-9337;

[63] S. Periyasamy, V. Gopalakannan, N. Viswanathan, Fabrication of magnetic particles imprinted cellulose based biocomposites for chromium (VI) removal, Carbohydrate polymers 174 (2017) 352-359;

[64] M. Luz, P. Ramos, J.A. Gonzalez, S.G. Albornoz, C.J. Perez, M.E. Villanueva, S.A. Giorgieri et all, Chitin hydrogel reinforced with TiO2 nanoparticles as an arsenic sorbent, Chem. Eng. J 285 (2016) 581-587;

[65] D. Zhao, X. Gao, C. Wu, R. Xie, S. Feng, C. Chen, Facile preparation of amino functionalized graphene oxide decorated with Fe3O4 nanoparticles for the adsorption of Cr (VI), Applied Surface Science 384 (2016) 1-9;

[66] T.D. Çiftçi, E. Henden, Nickel/nickel boride nanoparticles coated resin: A novel adsorbent for arsenic (III) and arsenic (V) removal, Powder Technology 269 (2016) 470-480;

[67] S. Yao, Z. Liu, Z. Shi, Arsenic removal from aqueous solutions by adsorption onto iron oxide/activated carbon magnetic composite, J. Environ. Heal. Sci. Eng. 12 (2014) 1-8;

[68] A. Hassan, A. Abdel-Mohsen, H. Elhadidy, Adsorption of arsenic by activated carbon, calcium alginate and their composite beads. Int. J. Biol. Macromol. 68 (2014a) 125–130;

[69] M. Bryjak, N. Kabay, B. L. Rivas, J. Bundschuh, Innovative materials and methods for water treatment: solutions for arsenic and chromium removal, (Eds.), CRC Press (2016) Vol. 2;

[70] J. Kamcev, M. K. Taylor, D. M. Shin, N. N. Jarenwattananon, K. A. Colwell, J. R. Long, Functionalized Porous Aromatic Frameworks as High-Performance Adsorbents for the Rapid Removal of Boric Acid from Water, Adv. Mater., 31(18) (2019) 1808027;

[71] M. Tanaka, Y. Takahashi, N. Yamaguchi, K. W. Kim, G. Zheng, M. Sakamitsu, The difference of diffusion coefficients in water for arsenic compounds at various pH and its dominant factors implied by molecular simulations. Geochim. et Cosmochimic. Acta, 105 (2013) 360-371;

[72] J. Antelo, M. Avena, S. Fiol, R. López, F. Arce, Effects of pH and ionic strength on the adsorption of phosphate and arsenate at the goethite–water interface, J. Colloid Interface Sci., 285(2) (2005) 476-486.